Northern High-Latitude Climate Changes During the Holocene as Simulated by Circulation Models

G. Lohmann

Alfred Wegener Institute for Polar and Marine Research, Bremerhaven, Germany

S.J. Lorenz

Max-Planck-Institute for Meteorology, Model and Data Group, Hamburg, Germany

M. Prange

DFG Research Center Ocean Margins, University of Bremen, Germany

To simulate the evolution of Holocene climate, forcing factors for the northern high-latitude climate are examined using different numerical models. A global coupled atmosphere–ocean circulation model driven by astronomical forcing over the last 7,000 years shows a long-term sea-surface temperature decrease in the Nordic Seas region associated with changes in seasonal insolation. A continuous cooling in the northeastern Atlantic is accompanied by a persistent warming in the Labrador Sea from the mid- to late Holocene. This temperature pattern can be attributed to a progressive weakening of the Icelandic Low and altered winds over the Nordic Seas induced by changes in insolation. In the early Holocene, important forcing for the Nordic Seas in the early Holocene was probably caused by melting land ice masses and "deepening" of the Bering Strait. The effects of meltwater discharge and Bering Strait inflow are studied in a regional model of the Arctic and North Atlantic Oceans. It is suggested that a gradual increase in the flux of Pacific water through the Bering Strait during the early Holocene slowly affected the polar climate by melting ice and causing ocean circulation changes in the Nordic Seas. This high-latitude response to sea level change is shown to be different from the signature obtained by a freshwater release linked to the final outburst drainage of Laurentide lakes.

1. INTRODUCTION

A number of different processes affected the climatic evolution of the Nordic Seas during the past 10,000 years (the Holocene). Since this time span comprises half a precessional cycle [*Milankovitch*, 1941], astronomical forcing is an important factor that has to be considered when studying Holocene climate variability. Other factors are linked to the melting of land ice. During the early Holocene, remnants of glacial ice sheets were still present in northeastern North America and Scandinavia [e.g., *Peltier*, 1994]. The melting of these ice sheets influenced the oceanic circulation not only by freshening the sea water (i.e. lowering sea-water density) but also by inducing eustatic and isostatic sea-level changes. In particular, a slowly increasing sea level allowed the reopening of the Bering Strait 12-13 kyBP (1,000 years before present). The Bering land-bridge inundation was

XXXXX
Geophysical Monograph Series XXX
Q1

10.1029/XXXGMXX

completed 5-6 kyBP [*Elias et al*., 1996]. The influence of post-glacial meltwater on ocean circulation was not always gradual. One particular abrupt event was presumably caused by a catastrophic release of freshwater into the Labrador Sea from the final outburst drainage of Laurentide lakes at about 8.2 kyBP, resulting in a weakening of the thermohaline circulation (THC) and a reduction in its northward heat transport [*Barber et al*., 1999].

Here, we present new modeling efforts designed to elucidate the particular roles of different parameters in forcing the Holocene climatic evolution of northern high latitudes. Two fully coupled climate models are employed to analyze the effects of orbital forcing and freshwater release from North America into the Labrador Sea. In addition, a regional ocean–sea-ice model is used to study the roles of reduced Bering Strait throughflow and enhanced freshwater input to the Arctic Ocean during the early Holocene.

Our model studies represent a first attempt to assess the relative importance of different forcing factors for the Holocene evolution of the Nordic Seas. They may help to interpret paleoceanographic records from that region.

2. METHODOLOGY

2.1. Global Climate Model: Varying Orbital Parameters

For the simulation of mid- to late Holocene climate changes owing to orbital forcing, we apply the coupled atmosphere-ocean general circulation model ECHO-G [*Legutke and Voss*, 1999]. The atmospheric part of this model is the circulation model ECHAM4 [*Roeckner et al*., 1996] with T30 horizontal resolution (approximately $3.8° \times 3.8°$) and 19 vertical levels. The ocean model includes a dynamic thermodynamic sea-ice model with snow cover and has a resolution of approximately $2.8° \times 2.8°$. The model consists of 20 irregularly spaced vertical levels with 10 levels covering the upper 300 m. The atmospheric model ECHAM4 has been modified with respect to the standard version to account for sub-grid scale partial ice cover [*Grötzner et al*., 1996], which is also considered in the ocean model component.

2.1.1. Orbital forcing. The ECHO-G model has been adapted to account for the influence of the annual distribution of solar radiation due to the slowly varying orbital parameters: the eccentricity of the Earth's orbit, the angle between the vernal equinox and the perihelion on the orbit, and the obliquity [*Milankovitch*, 1941]. The calculation follows *Berger* [1978] in providing the incoming solar radiation at the outer boundary of the atmosphere as a function of latitude and time.

The maximum deviation from present insolation was between 13.5 and 8.5 kyBP at the Northern Hemisphere summer. This is due to both a larger tilt of the Earth's rotation axis and the phase in the precession cycle, with the perihelion centered on the boreal summer solstice in the early Holocene. The insolation pattern in the Southern Hemisphere is much like that of the Northern Hemisphere, with a 10-ky phase shift (one half of the precessional cycle). At the winter solstice, a lack of insolation during the early to mid-Holocene compared to today is therefore south of the equator, which is mainly affected by the precession cycle, since the distance to the Sun is then at maximum in boreal winter. At 4.5 kyBP, the insolation at the top of the atmosphere roughly reached the present insolation distribution.

2.1.2. Experimental setup. For the control run, we utilize constant greenhouse gas concentrations typical for the preindustrial era (280 ppm CO_2, 700 ppb CH_4, and 265 ppb N_2O) and modern irradiance. This experiment has been integrated over 3,000 years of model simulation into a preindustrial climate state.

Computer resources for running a complex model like ECHO-G over the time period of the Holocene are very demanding. Therefore, the time scale of the orbital forcing has been shortened by an acceleration factor of 10, which implies that the response of the system to insolation forcing is completed after centuries. In effect, this procedure decouples any slowly responding portions of the system (e.g., deep-water properties) from the feedback structure.

The insolation trends of the last 7,000 years are represented in 700 model years. For the simulation of the Holocene climate we perform two experiments that differ in their initial conditions. For a detailed description of the procedure we refer to *Lorenz and Lohmann* [2004], where the effect of the acceleration factor on Holocene climate trends is evaluated. It is found that (within the model) the magnitude of orbitally forced Holocene trends is largely independent of the chosen acceleration factor.

2.2. Regional Model: Sea Level and Melting Arctic Ice Sheets

To examine the effects of Arctic meltwater discharge and Bering Strait throughflow on high-latitude ocean dynamics, we utilize the Coupled Ocean–Sea-ice Model with Open Surface (COSMOS) covering the Arctic Ocean, the Nordic Seas, and the Atlantic Ocean north of approximately 20 °S [*Prange*, 2003; *Prange and Lohmann*, 2003; *Prange and Gerdes*, 2004]. The model is formulated on a rotated grid to avoid the singularity of geographical coordinates at the pole (Figure 1) and has a horizontal resolution of about 100 km and 19 nonequidistant vertical levels. The ocean–sea-ice model is forced by atmospheric fields from a validated 15-year (1979-1993) period of the European Center for Medium-Range Weather Forecasts [*Prange*, 2003].

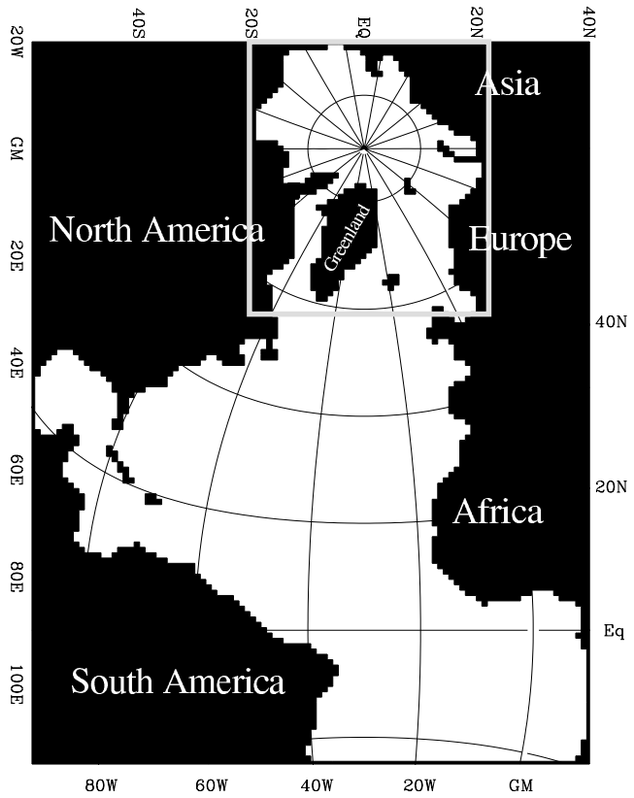

Figure 1. Domain of the regional model COSMOS. Both the geographical and the model grid coordinates are displayed. The frame marks the area that is shown in Figures 8-11.

In addition to atmospheric forcing, the ocean–sea-ice system is forced by river runoff and Bering Strait inflow. The river water inflow is implemented in the model as volume fluxes with zero salinity. Fourteen Arctic rivers are implemented as well as some additional ungauged runoff from the Arctic coastlines. For the Atlantic portion of the model domain, the eight largest rivers are included as well as the freshwater supply from Hudson Bay and the Baltic Sea, as described in *Prange* [2003]. Two experiments are performed, the setups of which differ in freshwater discharge and Pacific water inflow into the Arctic Mediterranean. These forcings refer to the present (control run) and the early Holocene (~10 kyBP).

2.2.1. Control run. A climatology for monthly discharge of the largest Arctic rivers and runoff from the Norwegian coast is applied in the model. Monthly varying inflow of Pacific water through the Bering Strait is implemented based on direct measurements [*Prange*, 2003]. Salinity of this inflow varies between 31.5 psu in September/October and 33.5 psu in March/April [*Roach et al*., 1995]. The annual mean volume flux amounts to 0.8 Sv. Taking a reference salinity of 35 psu (the salinity of the Atlantic water component in the Arctic Ocean), the annual freshwater flux into the Arctic Ocean due to the Bering Strait inflow is 1,800 km^3. Aside from being a source term in the Arctic Ocean freshwater budget, the Bering Strait inflow is associated with a heat supply during the summer months. The temperature rises by up to 4 °C in September, while winter temperatures (December-May) are at freezing for the salinity [*Roach et al*., 1995]. In COSMOS, the inflow of Pacific water through the Bering Strait is implemented by the open surface, i.e. the barotropic flow is taken into account [*Prange and Gerdes*, 2004]. This approach is justified by the strait's shallow depth (~50 m) relative to the thickness of the topmost model grid boxes (20 m).

2.2.2. Experiment 10 kyBP. At the beginning of the Holocene, remnants of glacial ice sheets were present in northeastern North America and Scandinavia [e.g., *Peltier*, 1994]. Numerical reconstructions suggest that the waning of the Laurentide ice sheet during the last stages of the deglaciation gave rise to a considerable flux of meltwater into the Arctic Ocean [*Licciardi et al*., 1999]. Part of this water entered the ocean via the Mackenzie River basin, another part came from the northern islands of the Canadian Archipelago. *Licciardi et al*. [1999] calculated freshwater fluxes derived from meltwater and precipitation runoff from North America. For the early Holocene (~10 kyBP) they found a total freshwater input to the Arctic Ocean of about 1,250 $km^3\ yr^{-1}$. Melting of the Fennoscandian ice sheet remnants provided freshwater to the Norwegian Coastal Current.

Beside the freshwater forcing from melting ice sheets, there is geological evidence for increased river discharge into the Arctic Mediterranean. *Sidorchuk et al*. [1999] reconstructed the paleohydrology of the Vychegda River from the grain size of channel deposits, paleochannel morphology, and paleolandscape features. The Vychegda River is a major tributary of the Northern Dvina, which flows into the Barents Sea. During the early Holocene, the river flow was slightly enhanced. The distribution of freshwater alginite (chlorococcalean algae) in marine sediment cores from the Eurasian continental margin indicates that the freshwater input to the Kara Sea was also enhanced around 10 kyBP [*Boucsein*, 2000].

A quantification of the increased freshwater inputs during the early Holocene is difficult and subject to considerable uncertainty. As an "educated guess", we presume runoff from the Norwegian coast as well as into the Barents and Kara Seas to be 25% higher than today. Extreme runoff, amounting to three times the modern one, is assumed from North American and northern Greenland coasts. Table 1 summarizes the freshwater forcing in our experiments.

Concerning the freshwater budget of the Arctic Sea, the enhanced runoff is partly compensated by a lesser inflow of

Table 1. Freshwater Input From Continents to the Arctic Ocean for the Present-Day Control Run and Experiment 10 kyBP. Units are $km^3\ yr^{-1}$.

Region	Present-day	10 kyBP
Norwegian coast	380	475
Barents Sea	452	565
Kara Sea	1,310	1,638
Laptev Sea	797	797
East Siberian Sea	195	195
North American/ North Greenland coasts	405	1,215
Total	**3,539**	**4,885**

low-saline Pacific water. The lower sea level during the early Holocene restricted the flow through the Bering Strait [*Elias et al*., 1996]. We assume the 10-kyBP Bering Strait inflow was half of the modern level.

2.3. Global Circulation Model: Release of Freshwater

To analyse the climatic effect of a catastrophic release of freshwater into the Labrador Sea, the coupled atmosphere–ocean circulation model ECHAM3/LSG [*Voss et al*., 1998] has been employed. The ocean model has a free surface and includes a thermodynamic sea-ice model. The coupled model has a horizontal resolution of about 5.6°.

2.3.1. Experiment FW. In the experiment, a large freshwater anomaly in the northern North Atlantic is released in equal parts to two grid points on the Canadian coast of the Labrador Sea. The experimental setup of this scenario is described elsewhere [*Schiller et al*., 1997; *Lohmann*, 2003]. The freshwater input to the Labrador Sea forces a transient shutdown of the THC, reducing the northward heat transport in the Atlantic Ocean. The circulation recovers completely after about 600 years, when the freshwater input was switched off [*Schiller et al*., 1997]. For our analyses, the model output of years 140-150 is taken. At this time, the overturning circulation was about 50% of its present-day value of 18 Sv ($1\ Sv = 1 \times 10^6\ m^3\ s^{-1}$).

3. RESULTS

3.1. ECHO-G: Orbitally Forced Climate Variations

The transient simulations performed with the ECHO-G coupled model, forced by Earth's orbital parameters, exhibit coherent surface temperature trends during the mid- to late Holocene (Figure 2). Regional temperature trends in the North Atlantic realm indicate both positive and negative values: A continuous cooling in the northeastern Atlantic is accompanied by a continuous warming in the region around the Labrador Sea and large areas in the subtropics. The orbitally induced signal of reduced boreal summer insolation in northern mid- and high latitudes (Figure 3) is reflected by a surface temperature drop of up to 2 degrees Kelvin (K) at high latitudes during the last 7,000 years. The most pronounced temperature trends occur over the continents. Enhanced warming during the Holocene occurs in the arid subtropical continents, from northern Africa via western Asia to the Indian subcontinent [*Lorenz and Lohmann*, 2004]. The most distinct cooling takes place over continental and sea-ice–covered northern high latitudes. We find that the trend is robust against the choice of ensemble members (not shown), indicating that the difference in the interannual variability of both experiments has no significant effect on the amplitude and distribution of the regional trends.

Motivated by the Palaeoclimate Modeling Intercomparison Project (PMIP) [*Joussaume and Taylor*, 1995], we take a snapshot of the mid-Holocene time slice at 6 kyBP (sometimes referred to as the Holocene climate optimum). PMIP has fostered a systematic evaluation of climate models, besides others, under conditions of the mid-Holocene. The time slice 6 kyBP was chosen to test the near-equilibrium response of climate models to orbital forcing with CO_2 at preindustrial concentration and present ice sheet distribution. Furthermore, we evaluate the time slices at 4 and 2 kyBP.

Our analyses are based on averages of 60 simulation years out of the set of two 700-year-long transient Holocene experiments, centered at 6, 4, and 0 kyBP. The largest orbitally forced temperature difference between the time slices occurs in the Arctic in October. The simulated near-surface temperature of the 6 kyBP climate for October is shown in Figure 4a, whereas Figure 4b displays temperature anomalies from the latest pre-industrial climate. Sea-ice thickness and its anomalies are also shown in Figure 4. A uniform warming of 3 to 6 K can be detected over the entire Arctic Ocean (Figure 4b), accompanied by a decrease of the Arctic sea-ice thickness of 40 to 80 cm (Figure 4d). The maximum anomalies are located near the New Siberian Islands and Franz Joseph Land. In these regions, the temperature anomaly exceeds 6 K and the sea-ice reduction amounts to more than 80 cm in the same areas. Note the reduction in sea-ice extent in the mid-Holocene simulation in Hudson Bay, the Greenland Sea, and the Barents and Bering Seas, compared with that at 0 kyBP (dark shaded area with sea-ice compactness of more than 20% for 6 kyBP in Figure 4c, and for 0 kyBP in Figure 4d).

The temperature change indicates a strong nonlinear signal in the model response to the radiative forcing: The upper ocean stores the heat of the boreal summer insolation, i. e. $30\ W\ m^{-2}$ more energy input than today in the Arctic from mid-June to the end of July (Figure 3a). The warmer sea-surface

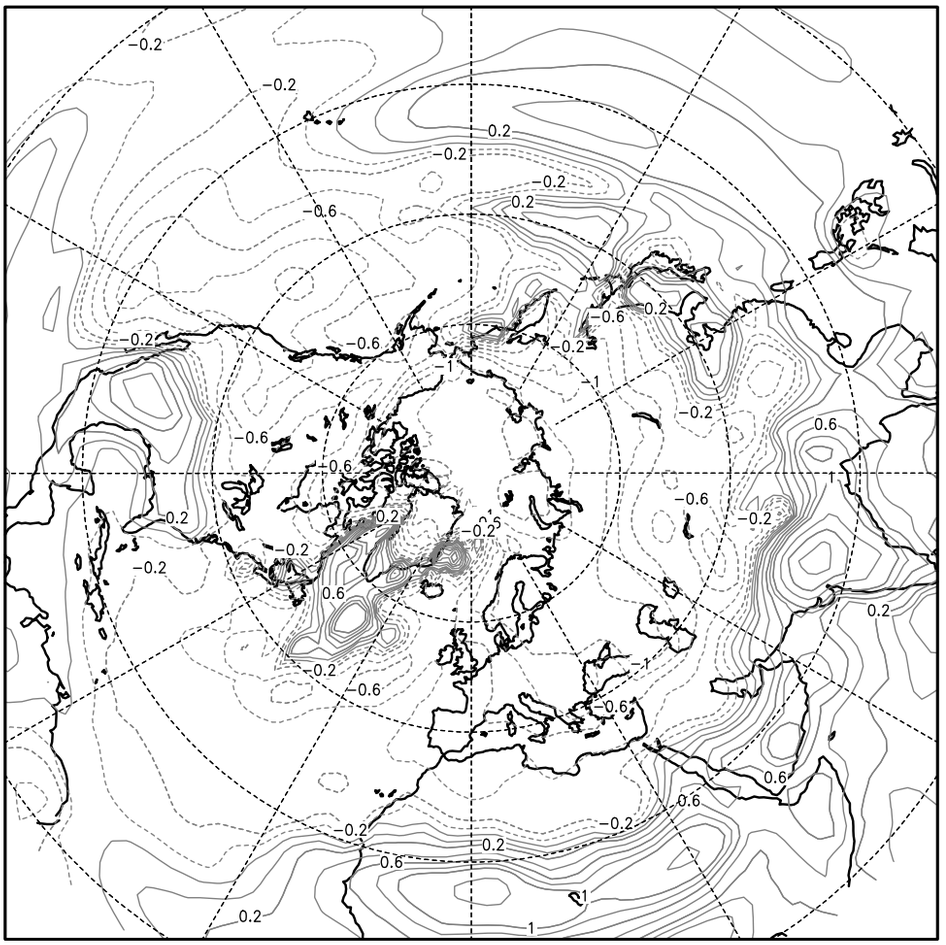

Figure 2. ECHO-G: Mean surface temperature trend from the mid-Holocene into the preindustrial era (7 to 0 kyBP) of the ensemble simulations using an acceleration factor of 10 (700 simulation years). The surface temperature is taken over open water, sea-ice, ground, and snow areas, respectively. Units are K (7 ky)$^{-1}$. Contour lines are at ±0.1, *0.2*, 0.4, *0.6*, 0.8, *1.0*, 1.5, *2.0*, 2.5, where the italicized numbers mark the labeled contour lines.

temperature (SST) during the summer season with high-level solar energy input lengthens the ice-free season and reduces the average sea-ice thickness in October, although the radiation anomaly has already turned its sign. The sea-ice/upper ocean introduces therefore a seasonally delayed response to the Milankovitch forcing. The situation is qualitatively similar for 4 kyBP (Figure 5) and 2 kyBP (not shown).

The model also simulates modified surface winds during the mid-Holocene boreal winter in the Arctic region (Figure 6). We find enhanced southward winds in the western part of the Greenland Sea and over the Denmark Strait. Furthermore, there is intensified cyclonic circulation in the Norwegian Sea. This is consistent with a stronger Icelandic Low during 6 kyBP relative to the preindustrial climate. For 4 kyBP (Figure 7), the enhanced southward winds remain, but the cyclonic circulation in the Norwegian Sea is reduced and shifted to the east. We have evaluated a North Atlantic Oscillation (NAO) Index by taking the pressure difference (in hPa) at sea level between the regions (50 °W to 50 °E, 60 °N to 80 °N) and (60 °W to 60 °E, 15 °N to 50 °N) as in *Felis et al*. [2004]. The modeled NAO trend is 1.5 hPa for 6,000 years, analogous to an NAO Index of 13.5, 13.0, 12.5, and 12.0 hPa for the time slices at 6, 4, 2, and 0 kyBP, respectively.

The wind effects change sea-ice dynamics and, in particular, enhance southward sea-ice transport along the eastern coast of Greenland during the mid-Holocene, consistent with findings of *Tremblay et al*. [1997]. This causes increased sea-ice concentration and a temperature drop southeast of Greenland. Along with the positive phase

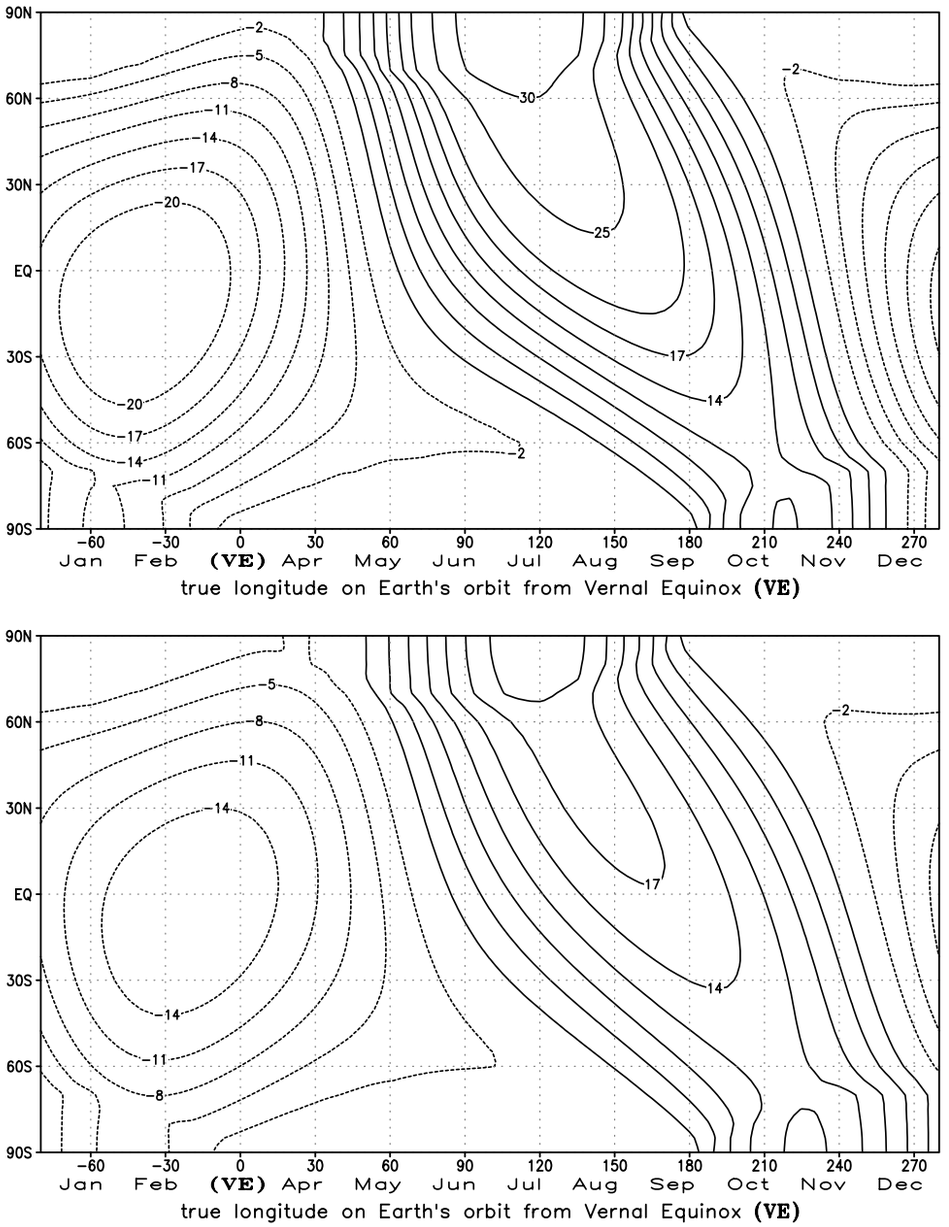

Figure 3. Solar insolation at 6 kyBP (top) and 4 kyBP (bottom) relative to the present. The calculation follows *Berger* (1978). Units are W m^{-2}.

of the NAO, a mid-Holocene temperature rise in Europe can be observed in the model results (Figure 2).

Between 4 and 2 kyBP, we find a warm phase widespread into the northern mid- to high latitudes, which is mainly located over the North American and Eurasian continents [*Lorenz and Lohmann*, 2004]. For 2 kyBP (not shown), the southward wind anomalies are absent and only an increased eastward component of the surface winds is detected. There is a strong temperature decrease in northern mid-latitudes between 7 and 4 kyBP for the boreal winter season and the annual mean [*Lorenz and Lohmann*, 2004].

3.2. COSMOS: Bering Strait and Meltwater Effects

The control run and the experiment 10 kyBP are started from the same spin-up run described by *Prange* [2003].

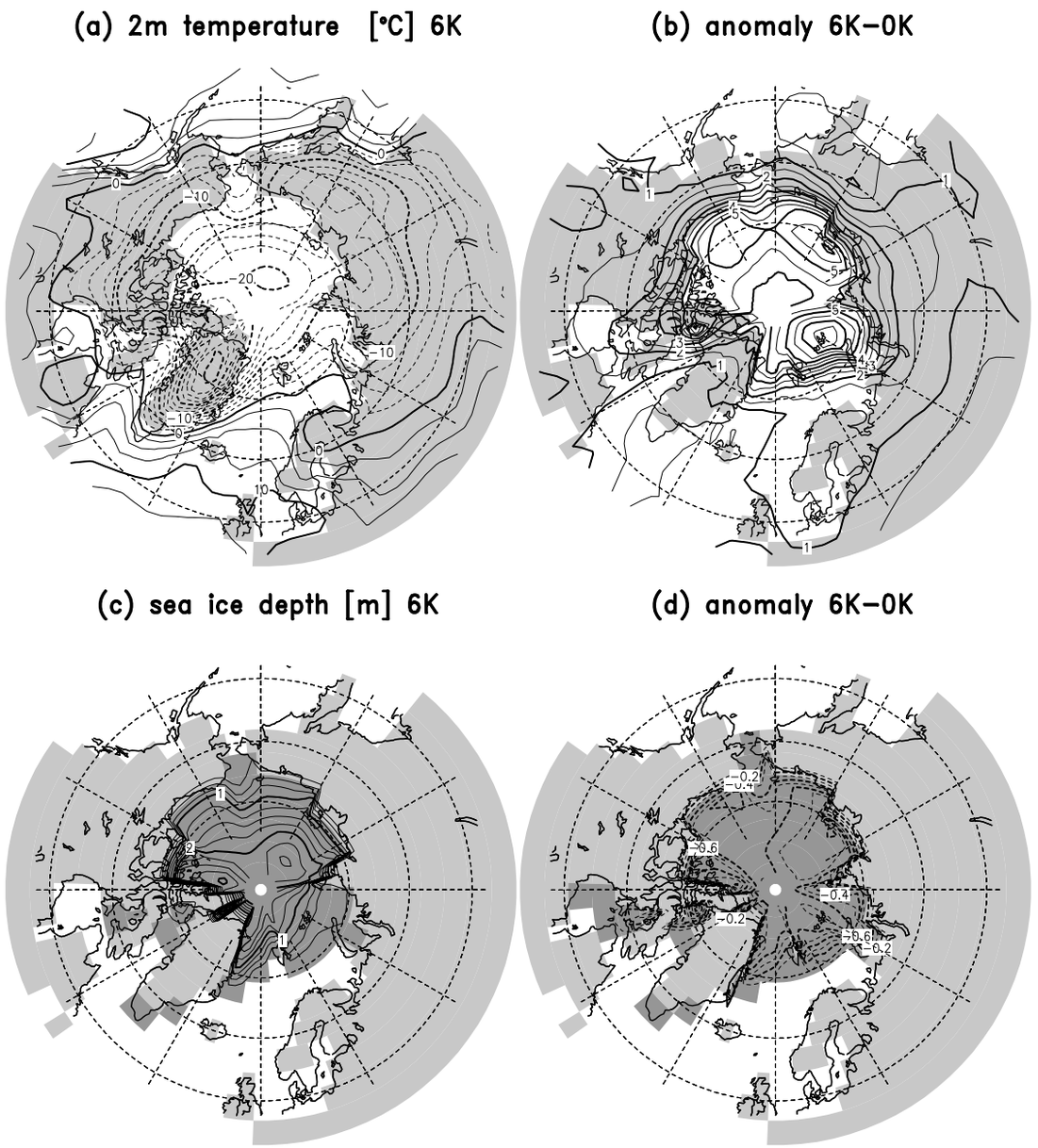

Figure 4. ECHO-G: Surface air temperature (a), sea-ice thickness and compactness (c) in October for the mid-Holocene climate at 6 kyBP; surface air temperature anomaly (b) of the mid-Holocene from the preindustrial climate and sea-ice thickness anomaly and sea-ice compactness (d). Areas where sea-ice compactness exceeds 20% are darkly shaded for 6 kyBP in (c) and for 0 kyBP in (d) (no anomaly). Light shading indicates continents in the T30 resolution of the atmospheric submodel ECHAM. Displayed is the mean of the two-700 year Holocene simulations for October, where 6 kyBP is a mean of 60 model years between 5.7 and 6.3 kyBP, and 0 kyBP is a similar average around the preindustrial climate. The contour intervals for temperature (sea-ice thickness) are 2.5 K (0.25 m) and 0.5 K (0.1 m) for anomalies, respectively.

For each experiment, the model is integrated for 60 years. In the following, we show annual mean fields that apply to the last year of the integration period (multi-year averaging is not necessary, since internal interannual variability proves to be negligible in the modeled Arctic Ocean).

3.2.1. Control experiment. The present-day (model-derived) ocean circulation averaged over the top 80 m in the polar and subpolar seas is presented in Figure 8. The top 80 m are represented by the three topmost levels of the model grid and comprise the surface mixed layer with the upper

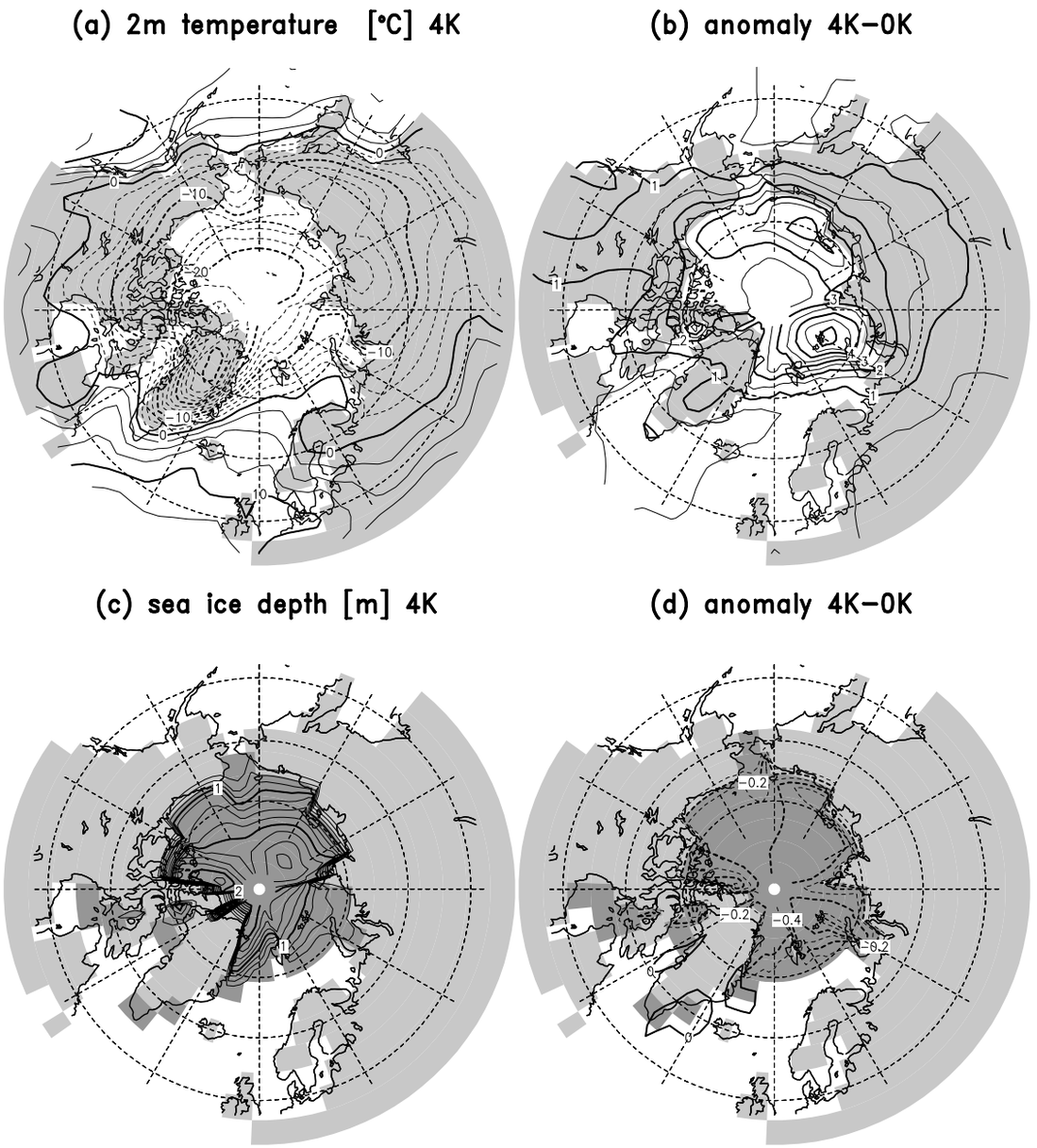

Figure 5. Same as Figure 4, but for 4 kyBP.

part of the cold halocline in the Arctic Ocean. A strong cyclonic gyre dominates the Nordic Seas, consisting of the East Greenland Current (EGC) in the west, and the Norwegian Atlantic Current (NAC) in the east. Atlantic water enters the Barents Sea, bringing some heat into the Arctic Ocean. This current constitutes the southern branch of an overall cyclonic flow pattern in the eastern Arctic Ocean. The Canadian Basin in the western Arctic is dominated by the anticyclonic Beaufort Gyre. The Transpolar Drift (TPD) carries polar waters towards the outlets of the Arctic Ocean, namely, the Fram Strait and the Nares Strait (Canadian Archipelago).

3.2.2. Experiment 10 kyBP. Figure 9 shows differences in upper ocean velocity between experiment 10 kyBP and the present-day control run. Over the Canadian Basin and the East Siberian Sea, the anticyclonic pattern is intensified. A cyclonic gyre north of Greenland and changes in the Eurasian Basin are associated with a modified path of the TPD. The reduced Bering Strait inflow is

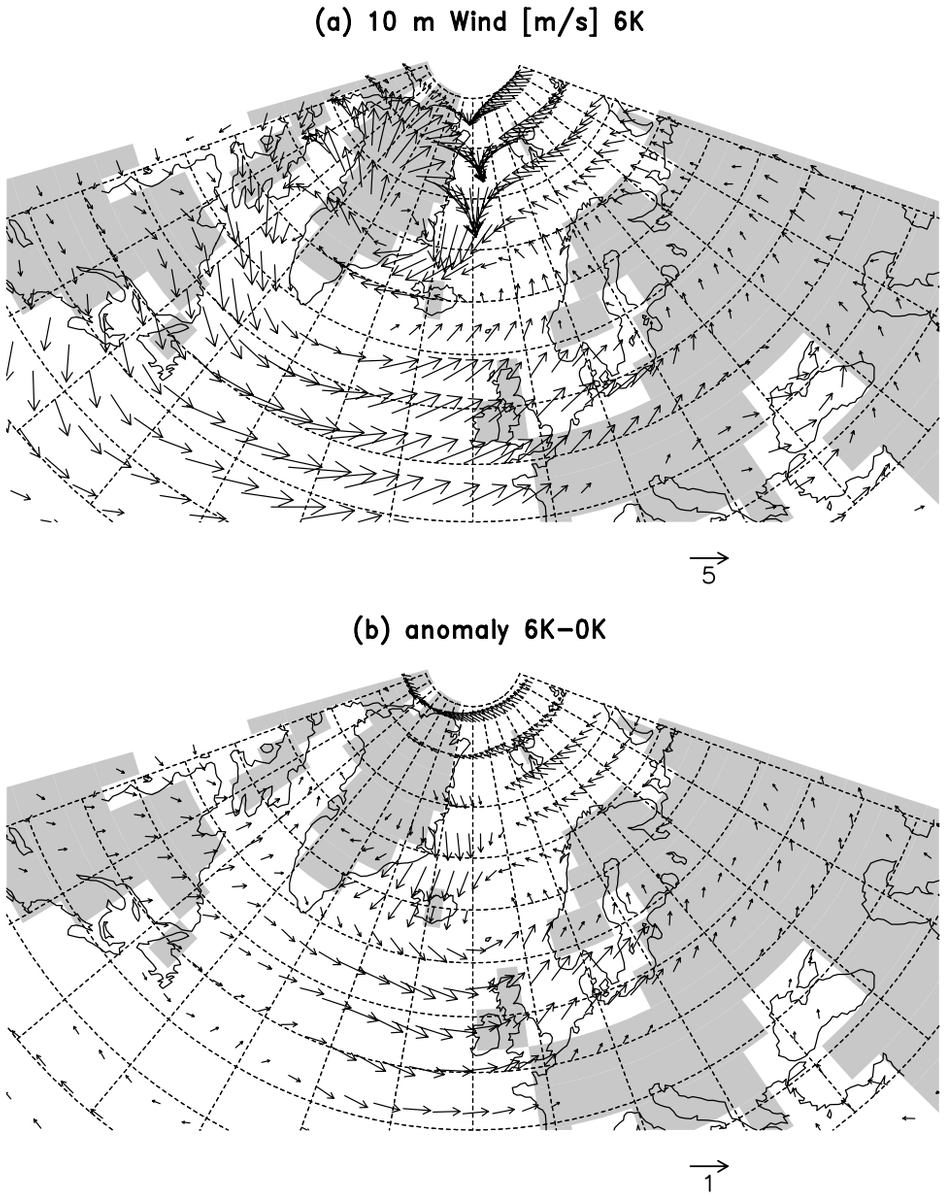

Figure 6. ECHO-G: (a) Surface wind during the boreal winter season (January to March) for the mid-Holocene climate at 6 kyBP. Vectors with a magnitude less than 1 ms^{-1} are suppressed. (b) Wind anomaly of the mid-Holocene from the preindustrial climate during the boreal winter season. Anomaly vectors less than 0.2 ms^{-1} are suppressed. As in Figure 4, the surface winds represent ensemble means of 60 model years averages.

compensated by a weaker outflow through the Canadian Archipelago and an increased inflow via the Barents Sea, maintaining a steady Arctic Ocean mass balance. In the center of the Nordic Seas, an anomalous cyclonic flow pattern is found.

Figure 10 presents annual mean differences between experiment 10 kyBP and the control run. The decreased heat input due to a reduced Bering Strait inflow in Experiment 10 kyBP causes sea-ice to be thicker by up to 1 m in the vicinity of the strait. This thick sea-ice is advected into the central Arctic. In conjunction with lowered heat fluxes from the ocean (not shown) owing to a stronger salinity stratification, this results in a thicker ice cover over wide areas of the Arctic Ocean and in the Greenland Sea. The drift of sea-ice is coupled with ocean currents through ocean–sea-ice stresses. Therefore, differences in sea-ice motion between

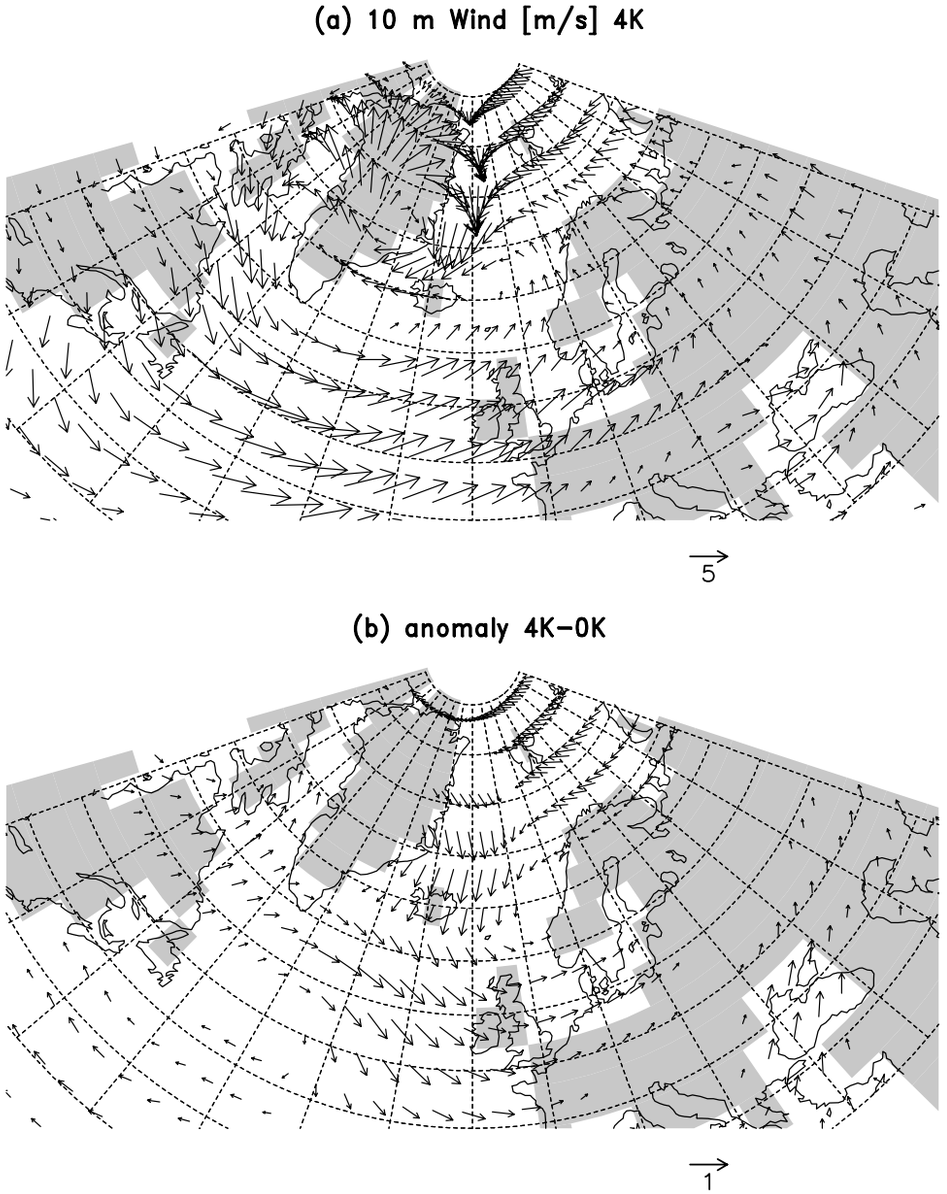

Figure 7. Same as Figure 6, but for 4 kyBP.

experiment 10 kyBP and the control run are almost identical to differences in the upper ocean circulation (see Figure 9).

Changes in the circulation are associated with changes in the field of upper ocean salinity. The meltwater from the Canadian coast is advected by the Beaufort Gyre into the central Arctic. Since the Bering Strait inflow is reduced, part of this freshwater can readily enter the Chukchi and East Siberian Seas. Lowered surface salinities in the Kara, Barents, and Norwegian Seas are directly caused by enhanced local runoff (see Table 1). The eye-catching high-salinity tongue north of Greenland (Figure 11a) results from the reduced inflow of low-saline Pacific water and a changed circulation pattern (Figure 9). Note also the low salinity in the EGC.

Differences in mean potential temperature between experiment 10 kyBP and the control run are presented in Figure 11b for the depth range 80-250 m. Largest values naturally appear in the "high-temperature" North Atlantic. But also in the Arctic Ocean we find differences up to 1 °C. In the central Arctic, these differences can be explained by changes in salinity (i.e., density) stratification rather than

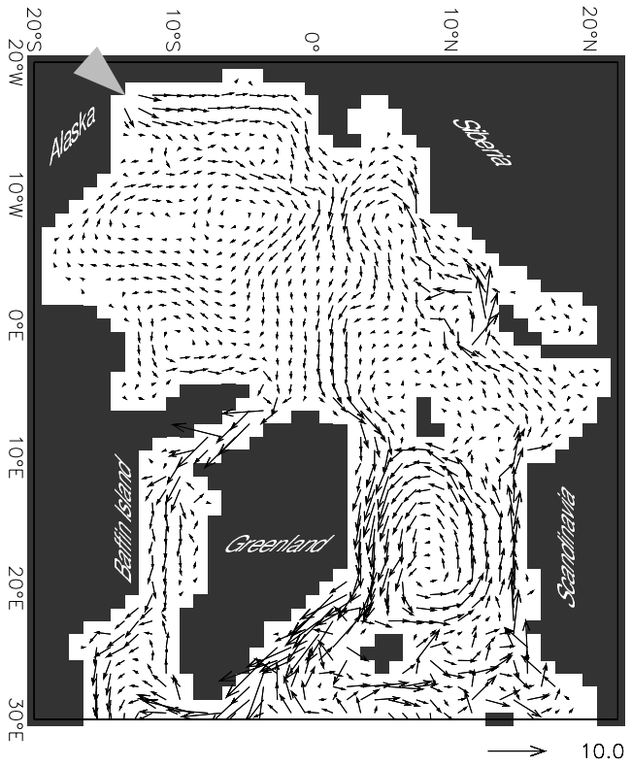

Figure 8. COSMOS: Annual mean upper ocean velocity (averaged over 0-80 m) in the present-day control run. Units are cm s^{-1}. Labels refer to the rotated model grid. The grey arrow marks the position of the Bering Strait.

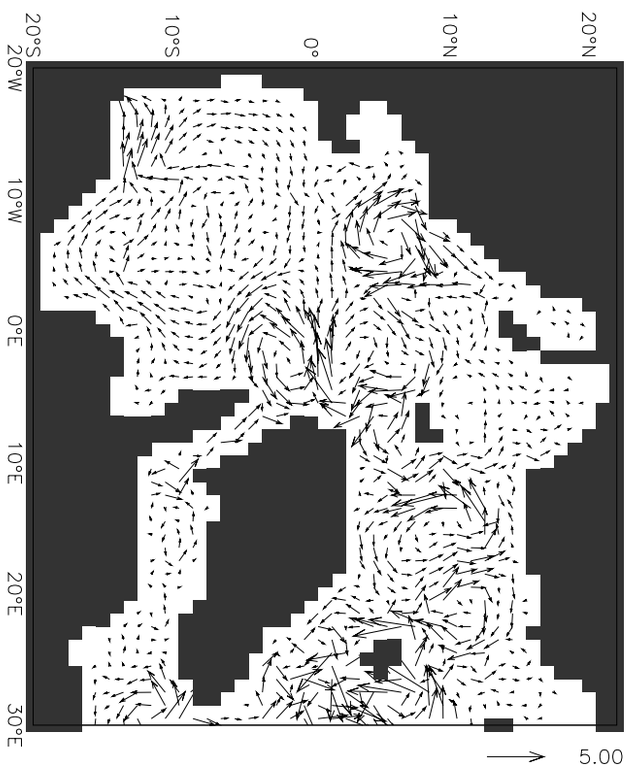

Figure 9. COSMOS: Difference in mean upper ocean velocity (averaged over 0-80 m) between experiment 10 kyBP and the present-day control run. Units are cm s^{-1}.

by horizontal advection. Low surface salinities stabilize the water column, thereby inhibiting convective mixing of cold surface water with warmer water from deeper halocline layers.

In the central Nordic Seas we find overall cooler conditions in experiment 10 kyBP compared with those in the control run. Along the Scandinavian coast and in the EGC, as well as northeast of Iceland, subsurface temperatures are higher.

3.3. ECHAM3/LSG: Freshwater Release

Caused by the freshwater release to the North Atlantic, the THC slows to 9 Sv and the northern North Atlantic cools considerably (Figure 12), where the strongest cooling is over the Nordic Seas caused by advanced sea-ice cover. Figure 13a shows surface winds during the freshwater release for the boreal winter season. We find enhanced southward winds in the Greenland Sea, over the Denmark Strait, and south of Greenland (Figure 13b) that favor the transport of polar water masses into the North Atlantic.

4. DISCUSSION

The impact of the distribution of incident solar radiation on the Holocene climate is investigated by using a coupled atmosphere–ocean–sea-ice model. Justified by the much longer time scale of the astronomical forcing than that of the dynamical feedback processes in the atmosphere-ocean system, we accelerate the time scale of the orbitally varying solar radiation by a factor of 10. This enables the simulation of the mid- to late Holocene climatic evolution in northern high latitudes with a complex circulation model.

This method is limited to the investigation of long-term effects on the atmosphere–ocean–sea-ice system caused by the astronomical forcing. We find no significant changes in the THC in the simulations [*Lorenz and Lohmann*, 2004], nor is our model designed to resolve deep ocean circulation changes.

Based on model simulations that are forced solely by insolation, the surface temperature trend shows a spatial pattern consistent with a weakening of the Icelandic Low from the mid- to late Holocene. The modeled temperature and wind patterns reflect a strong response to a gradual insolation

Figure 10. COSMOS: Difference in mean sea-ice thickness between experiment 10 kyBP and the present-day control run. Units are m.

forcing (Figure 3). A strong Icelandic Low (positive NAO phase) is accompanied by a relatively mild winter over northern Europe. The information about the winter circulation is stored in the subsurface while the summer signal is destroyed in the following winter. Therefore, the annual mean SST response to changes in the atmospheric circulation is almost identical to the winter signal in the NAO. It is therefore not astonishing that the cold season signal is preserved in the reconstructed SSTs. Indeed, alkenone SST reconstructions in the northeastern Atlantic show strong negative SST trends for 6 kyBP relative to the preindustrial climate, 4.4 K at 75 °N,14 °E [*Marchal et al*., 2002], 1.79 K at 67 °N,8 °E [*Calvo et al*., 2002], and 3.26 K at 58 °N,9 °E [*Emeis et al*., 2003], whereas a core further east, at 59 °N,26 °W [*Marchal et al*., 2002], shows a moderate cooling of 0.62 K within 6,000 years only. These data are consistent with a recent analysis of alkenone SST reconstructions, which shows that negative SST trends in the northeastern Atlantic and western Mediterranean, along with positive SST trends in the eastern Mediterranean, northern Red Sea, and western subtropical Atlantic, are connected with a continuous weakening of the NAO pattern from the early to late Holocene [*Rimbu et al*., 2003]. The northern hemisphere extratropical response is linked to Rossby wave propagation from low latitudes during the boreal winter. This relationship is also consistent with a global set of collected marine proxy temperature data

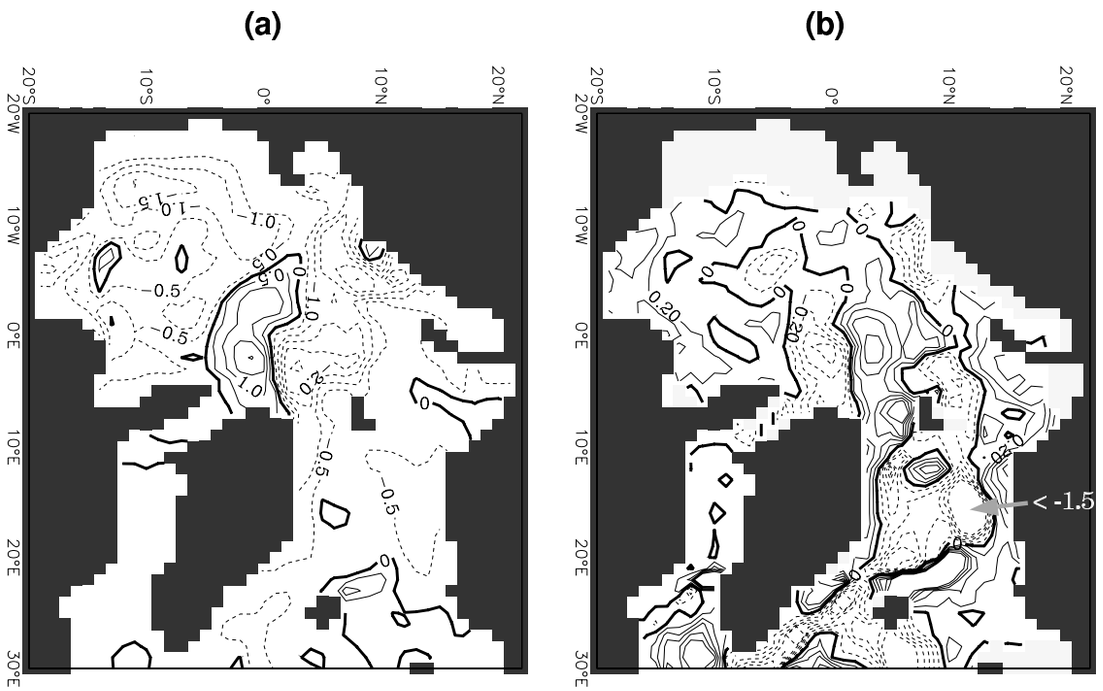

Figure 11. COSMOS: Difference in mean hydrographic fields between experiment 10 kyBP and the present-day control run (i.e., 10 kyBP minus present-day). (a) Salinity averaged over 0-80 m. (b) Potential temperature averaged over 80-250 m. Contour interval is 0.2 °C.

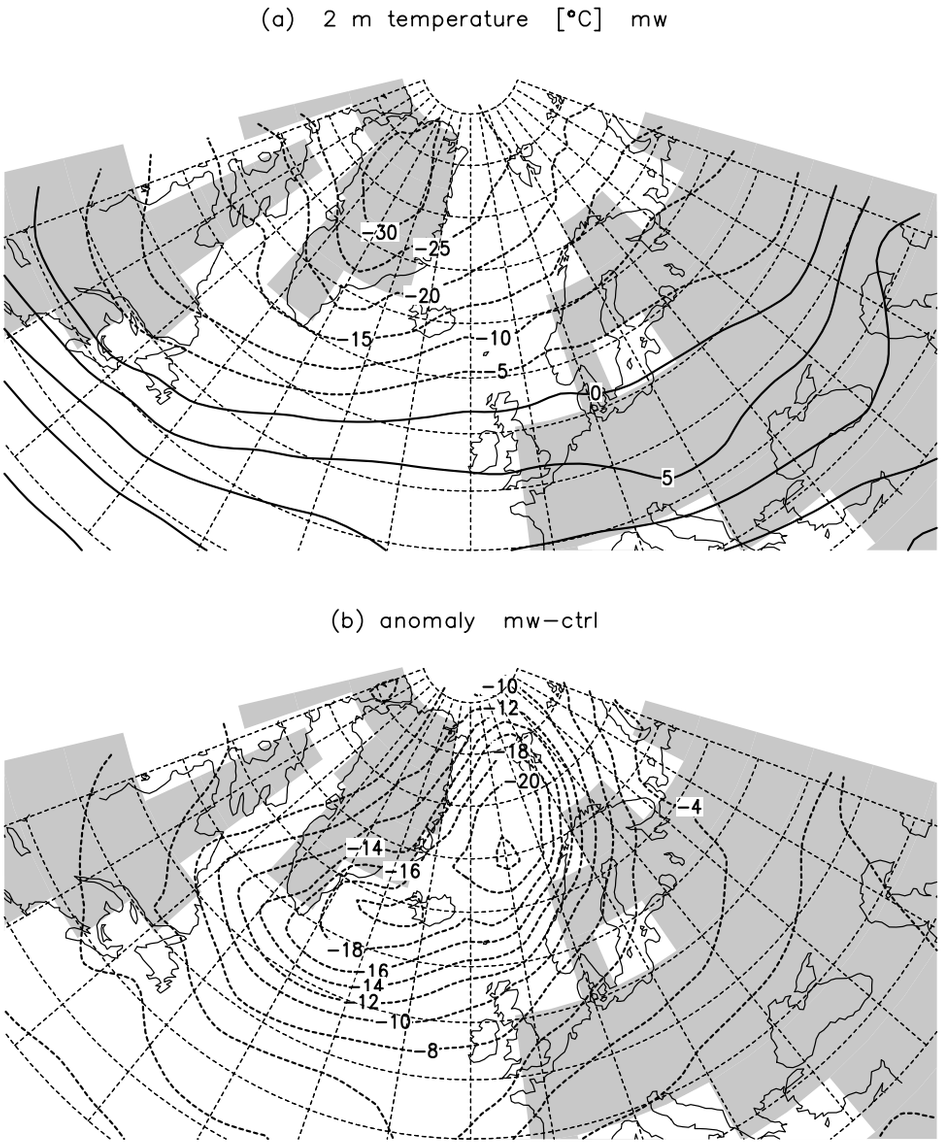

Figure 12. ECHAM3/LSG: a) Near-surface air temperature during the freshwater release for the boreal winter season (January to March). (b) Anomaly from the control integration.

[*Emeis et al*., 2000; *Marchal et al*., 2002; *Rohling et al*., 2002]. A coherent picture of neoglaciation since 7 kyBP is revealed by the model and proxy data: Opposite trends of warming and cooling occur in the tropics and mid-latitudes [*Rimbu et al*., 2004; *Lorenz et al*., 2005]. The pronounced warming at 6 kyBP in the Arctic Ocean as seen in the experiments is supported by proxy data [*Texier et al*., 1997; *Andreev et al*., 2001] and a northward shift of the Arctic tree lines [*Tarasov et al*., 1998]. Driftwood records reveal increased Fram Strait outflow by around 6 kyBP [*Dyke et al*., 1997; *Tremblay et al*., 1997]. *Prange and Lohmann* [2003] pointed out the importance of freshwater input by Arctic rivers on the Arctic upper ocean and sea-ice circulation. Changes in wind direction may also affect the path of the TPD and ice export from the Arctic which is led to further investigations.

Furthermore, the effect of a freshwater release into the Labrador Sea is shown for present-day background conditions mimicking a perturbation induced by the final outburst drainage of Laurentide lakes at about 8.2 kyBP [*Alley et al*., 1997]. Although a direct comparison with the simulations for the effect of Earth's orbital parameters (section 3.1) is not possible due to another model and model resolution, it

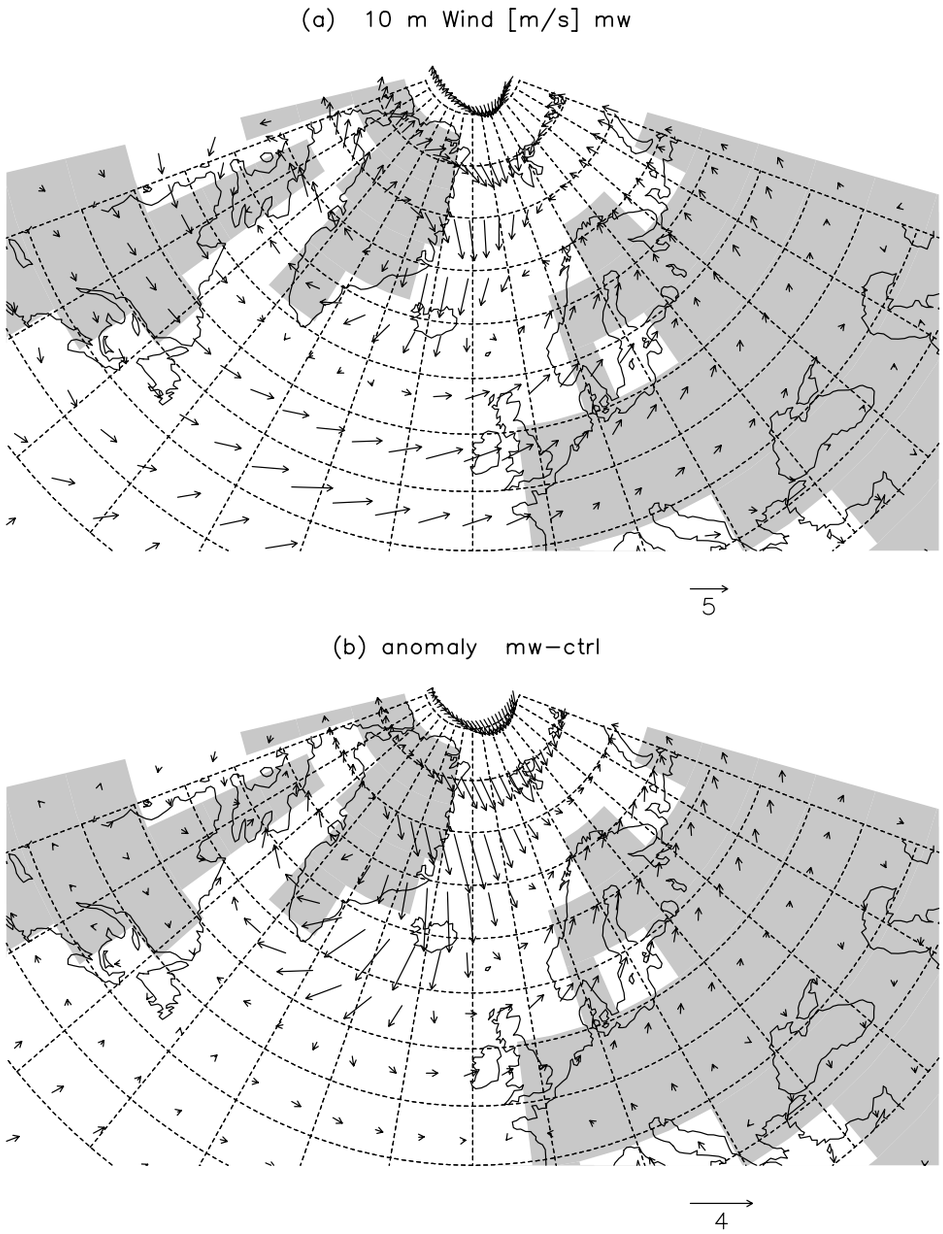

Figure 13. ECHAM3/LSG: (a) Surface wind during the freshwater release for the boreal winter season (January to March). (b) Wind anomaly from the control integration. Units are m s^{-1}.

can be seen that the sudden freshwater input (Figure 13b) has a stronger effect on climate than the gradual Milankovitch forcing for 6 kyBP (cf. Figure 6b).

5. CONCLUDING REMARKS

To avoid the necessity of prescribed SST, coupled atmosphere–ocean simulations of the mid-Holocene climate [*Texier et al*., 1997; *Hewitt and Mitchell*, 1998; *Voss and Mikolajewicz*, 2001; *Kitoh and Murakami*, 2002] have recently been performed. These experiments simulate near-equilibrium states of the mid-Holocene climate (6 kyBP) or perform a series of time slices stepping through the Holocene [*Liu et al*., 2003]. *Liu et al*. [2003] applied the time slice concept and also found a cooling at low latitudes and a warming at higher latitudes during the mid-Holocene and attributed this to direct radiation changes. Our method can also be used to obtain the climate at certain time intervals at optimal computing

costs [*Lorenz and Lohmann*, 2004; *Felis et al*., 2004]. In our experiments, we detect changed winds during the mid- to late Holocene in the Nordic Sea region associated with the strength and position of the Icelandic Low and related westward winds. Our study indicates changes in the strength of the Icelandic Low with a significant trend on multi-millenial time scales (1.5 hPa for 6,000 years). Induced by anthropogenic greenhouse gases in the atmosphere, we found with the same model an increase for the modeled index is about 1.7 hPa within the last hundred years [*Felis et al*., 2004], indicating that the effect of the increased greenhouse gases in the atmosphere on the strength of the Icelandic Low is of similar magnitude than the effect linked to the orbital parameters.

We find a strong warming in the Barents Sea for 6 kyBP to 2 kyBP relative to the preindustrial climate. Interestingly, the anomalous southward component of surface winds in the Nordic Seas at 6 kyBP and 4 kyBP is absent for the 2 kyBP climate. Such nonlinear variations in wind field affect the Holocene hydrography in the Nordic Seas as will be discussed in forthcoming studies. In our experimental setup, we have neglected interactions with changes in vegetation cover which may be of particular importance for the snow cover over land [*Ganopolski et al*., 1998] and for permafrost [*Velichko et al*., 1995]. Future model configurations will elaborate vegetation–climate feedbacks and permafrost effects in our framework for Holocene climate modeling.

To simulate the climate of the early Holocene, freshwater fluxes from melting ice sheets and topographic changes have to be taken into account. Our regional model shows that these processes may have an important influence on high-latitude ocean and sea-ice dynamics. In our experiments, we find a substantial effect on the strength and size of the Beaufort Gyre, which is corroborated by geological evidence. On the basis of the heavy-mineral distributions in Arctic Ocean sediment cores, *Behrends* [1999] reconstructed paleo–sea-ice drift patterns. The data suggest that the Beaufort Gyre expanded during the early Holocene.

An important implication of the gradual Bering Strait deepening in the course of the early Holocene is the increasing heat flux into the Arctic Ocean. Our regional model shows that the inflowing heat exerts a strong influence on polar sea-ice. An intensified warm Bering Strait inflow causes a decline in sea-ice coverage in the Chukchi and East Siberian Seas. Where sea-ice is replaced by open water, the surface albedo substantially decreases. It is therefore likely that the gradually increasing influx of Pacific water during the early Holocene slowly affected the polar climate, raising local air temperatures.

Acknowledgments. We appreciate the constructive comments by Wolfgang Berger. This work was supported by Bundesministerium für Bildung und Forschung through DEKLIM, and by Deutsche Forschungsgemeinschaft through DFG Research Centre Ocean Margins at Bremen University (No. RCOM0140).

REFERENCES

Alley, R.B., T. Sowers, P.A. Mayewski, M. Stuiver, K.C. Taylor, P.U. Clark, Holocene climatic instability: A prominent, widespread event 8200 yr ago, *Geology*, 25, 483-486, 1997.

Andreev, A.A., V.A. Klimanov, and L.D. Sulerzhitsky, Vegetation and climate history of the Yana River lowland, Russia, during the last 6400yr, *Quat. Res*., 20, 259-266, 2001.

Barber, D.C., A. Dyke, C. Hillaire-Marcel, A.E. Jennings, J.T. Andrews, M.W. Kerwin, G. Bilodeau, R. McNeely, J. Southon, M.D. Morehead, J.-M. Gagnon, Forcing of the cold event of 8,200 years ago by catastrophic drainage of Laurentide lakes. *Nature*, 400, 344-348, 1999.

Behrends, M., Rekonstruktion von Meereisdrift und terrigenem Sedimenteintrag im Spätquartär: Schwermineralassoziationen in Sedimenten des Laptev-See-Kontinentalrandes und des zentralen Arktischen Ozeans. *Rep. Polar Res*., 310, Alfred-Wegener-Institute for Polar and Marine Research, Bremerhaven, 167 pp., 1999.

Berger, A.L., Long-term variations of daily insolation and Quaternary climatic changes, *J. Atmos. Sci*., 35, 2362-2367, 1987.

Boucsein, B., Organic carbon in Late Quaternary sediments: Responses to paleoenvironmental changes in the Laptev and Kara Seas (Arctic Ocean). *Rep. Polar Res*., 365, Alfred-Wegener-Institute for Polar and Marine Research, Bremerhaven, 103 pp., 2000

Calvo, E., J. Grimalt, and E. Jansen, High resolution U_{37}^{K} sea surface temperature reconstruction in the Norwegian Sea during the Holocene, *Quat. Sci. Rev*., 21, 1385-1394, 2002.

Dyke, A.S., J. England, E. Reimnitz, and H. Jette, Changes in driftwood delivery to the Canadian Arctic Archipelago: the hypothesis of postglacial oscillations of the Transpolar Drift. *Arctic*, 50, 1-16, 1997.

Elias, S.A., S.K. Short, C.H. Nelson, and H.H. Birks, Life and times of the Bering Land Bridge. *Nature*, 382, 61-63, 1996.

Emeis, K.-C., U. Struck, H.-M. Schulz, R. Rosenberg, S. Bernasconi, H. Erlenkeuser, T. Sakamoto, and F. Martinez-Ruiz, Temperature and salinity variations of mediterranean sea surface waters over the last 16,000 years from records of planktonic stable oxygen isotopes and alkenone unsaturation ratios, *Palaeogeogr. Palaeoclimatol. Palaeoecol*., 158, 259-280, 2000.

Felis, T., G. Lohmann, H. Kuhnert, S. Lorenz, D. Scholz, J. Pätzold, S.A. Al-Rousan, and S.M. Al-Moghrabi, Increased seasonality in Middle Eastern temperatures during the last interglacial period. *Nature,* 429, 164-168, 2004.

Ganopolski, A., C. Kubatzki, M. Claussen, V. Brovkin, and V. Petoukhov, The influence of vegetation-atmosphere-ocean interaction on climate during the mid-Holocene, *Science*, 280, 1916-1919, 1998.

Grötzner, A., R. Sausen, and M. Claussen, The impact of sub-grid scale sea-ice inhomogeneities on the performance of the atmospheric general circulation model ECHAM3, *Climate Dyn*., 12, 477-496, 1996.

Hewitt, C.D. and J.F.B. Mitchell, A fully coupled GCM simulation of the climate of the mid-Holocene, *Geophys. Res. Lett*., 25, 361-364, 1998.

Joussaume, S. and K.E. Taylor, Status of the Paleoclimate Modeling Intercomparison Project (PMIP), in *Proceedings of the First*

International AMIP Scientific Conference, vol. 92, pp. 425-430, WCRP, 1995.

Kim, J.-H., N. Rimbu, S.J. Lorenz, G. Lohmann, S.-I. Nam, S. Schouten, C. Rühlemann, and R. R. Schneider, North Pacific and North Atlantic sea-surface temperature variability during the Holocene. *Quat. Sci. Rev*., 23, 2141-2154, 2004.

Kitoh, A. and S. Murakami, Tropical Pacific climate at the mid-Holocene and the Last Glacial Maximum simulated by a coupled atmosphere-ocean general circulation model, *Paleoceanography*, 17, doi:10.1029/2001PA000,724, 2002.

Legutke, S. and R. Voss, The Hamburg atmosphere-ocean coupled circulation model ECHO-G, *Technical Report* 18, Deutsches Klimarechenzentrum, Hamburg, Germany, 1999.

Licciardi, J.M., J.T. Teller, and P.U. Clark, Freshwater routing by the Laurentide Ice Sheet during the last deglaciation. In: *Mechanisms of global climate change at millennial time scales*. Edited by P.U. Clark, R.S. Webb, L.D. Keigwin, American Geophysical Union, Geophys. monograph series, No. 112, 177-201, 1999.

Liu, Z., E. Brady, and J. Lynch-Stieglitz, Global ocean response to orbital forcing in the Holocene, *Paleoceanography*, 18, 1041, doi:10.1029/2002PA000,819, 2003.

Lohmann, G., Atmospheric and oceanic freshwater transport during weak Atlantic overturning circulation, *Tellus*, 55 *A*, 438-449, 2003.

Lorenz, S., and G. Lohmann, Acceleration technique for Milankovitch type forcing in a coupled atmosphere-ocean circulation model: method and application for the Holocene. *Clim. Dyn*., 23, 727-743. DOI: 10.1007/s00382-004-0469-y, 2004.

Lorenz, S.J., J.-H. Kim, N. Rimbu, R.R. Schneider, and G. Lohmann, Orbitally driven insolation forcing on Holocene climate trends: evidence from alkenone data and climate modeling, *Paleoceanogr*., 2005, submitted.

Marchal, O., *et al*., Apparent long-term cooling of the sea surface in the northeast Atlantic and Mediterranean during the Holocene, *Quat. Sci. Rev*., 21, 455-483, 2002.

Milankovitch, M., *Kanon der Erdbestrahlung und seine Anwendung auf das Eiszeitenproblem*, 133, Royal Serb. Acad. Spec. Publ., Belgrad, 1941.

Peltier, W.R., Ice Age paleotopography. *Science*, 265, 195-201, 1994.

Prange, M., Einfluss arktischer Süβwasserquellen auf die Zirkulation im Nordmeer und im Nordatlantik in einem prognostischen Ozean-Meereis-Modell. *Report Polar Marine Res*., 468, Alfred-Wegener-Institute for Polar and Marine Research, Bremerhaven, 220 pp., 2003.

Prange, M. and G. Lohmann, Effects of mid-Holocene river runoff on the Arctic ocean-sea ice system: a numerical study. *The Holocene*, 13 (3), 335-342, 2003.

Prange, M. and R. Gerdes, The role of surface freshwater flux boundary conditions in Arctic ocean/sea-ice models, *J. Geophys. Res*., 2004 (submitted).

Rimbu, N., G. Lohmann, J.-H. Kim, H.W. Arz, and R.R. Schneider, Arctic/North Atlantic Oscillation signature in Holocene sea surface temperature trends as obtained from alkenone data, *Geophys. Res. Lett*., 30, 1280-1283, 2003.

Rimbu, N., G. Lohmann, S.J. Lorenz, J.-H. Kim, and R. Schneider, Holocene climate variability as derived from alkenone sea surface temperature reconstructions and coupled ocean-atmosphere model experiments. *Climate Dyn*., 23, 215-227, 2004.

Roach, A.T., K. Aagaard, C.H. Pease, S.A. Salo, T. Weingartner, V. Pavlov, and M. Kulakov, Direct measurements of transport and water properties through the Bering Strait. *J. Geophys. Res*., 100, 18443-18457, 1995.

Roeckner, E., *et al*., The atmospheric general circulation model ECHAM-4: Model description and simulation of the present-day climate, *Report* 218, Max-Planck-Institut für Meteorologie, 1996.

Rohling, E., P. Mayewski, R. Abu-Zied, J. Casford, and A. Hayes, Holocene atmosphere-ocean interactions: records from Greenland and the Aegean Sea, *Climate Dynamics*, 18, 573-592, 2002.

Schiller, A., U. Mikolajewicz, and R. Voss, The stability of the thermohaline circulation in a coupled ocean-atmosphere general circulation model. *Climate Dyn*., 13, 325-347, 1997.

Sidorchuk, A.Y., O.K. Borisova, N.N. Kovalyukh, A.V. Panin, A.V. Chernov, Paleogidrologiya nizhney Vychegdy v pozdneled-nikov'ye i v golotsene (Paleohydrology of the lower Vychegda in the late glacial period and Holocene). Vestnik Moskovskogo Universiteta, Seriya 5: *Geografiya*, 1999/5, 35-42, 1999.

Tarasov, P., *et al*., Present-day and mid-holocene biomes reconstructed from pollen and plant macrofossil data from the former Soviet Union and Mongolia, *Journal of Biogeography*, 25, 1029-1053, 1998.

Texier, D., N. de Noblet, S.P. Harrison, A. Haxeltine, D. Jolly, S. Joussaume, F. Laarif, I.C. Prentice, and P. Tarasov, Quantifying the role of biosphere-atmosphere feedbacks in climate change: coupled model simulations for 6000 years BP and comparison with palaeodata for northern Eurasia and northern Africa, *Climate Dyn*., 13, 865-882, 1997.

Tremblay, L.-B., L. Mysak, and A. Dyke, Evidence from driftwood records for century-to-millennial scale variations of the high latitude atmospheric circulation during the Holocene, *Geophys. Res. Lett*., 24, 2027-2031, 1997.

Velichko, A.A., O.K. Borisova, E.M. Zelikson, and V.P. Nechayev, Permafrost and vegetation response to global warming in North Eurasia. In: *Biotic feedbacks in the global climatic system*. Edited by G.M. Woodwell, F.T. Mackenzie, Oxford Univ. Press, New York, 134-156, 1995.

Voss, R., R. Sausen, and U. Cubasch, Periodically-synchronously coupled integrations with the atmosphere-ocean general circulation model ECHAM3/LSG. *Climate Dyn*., 14, 249-266, 1998.

Voss, R. and U. Mikolajewicz, The climate of 6000 years BP in near-equilibrium simulations with a coupled AOGCM, *Geophys. Res. Lett*., 28, 2213-2216, 2001.

G. Lohmann, Alfred Wegener Institute for Polar and Marine Research, Bussestrasse 24, D-27570 Bremerhaven, Germany. (lohmann@awi-bremerhaven.de)

S.J. Lorenz, Max-Planck-Institute for Meteorology, Model & Data Group, Bundesstr. 55, 20146 Hamburg, Germany. (lorenz@dkrz.de)

M. Prange, University of Bremen, Research Center Ocean Margins, P.O. 330 440, 28334 Bremen, Germany. (mprange@palmod.uni-bremen.de)

Query

Q1. Please provide copyright block.